

CAPILLARY-GRAVITY WAVES ON THE INTERFACE OF TWO DIELECTRIC FLUID LAYERS UNDER NORMAL ELECTRIC FIELDS

by A. Doak

(*Department of Mathematical Sciences, University of Bath, Bath BA2 7AY*)

T. Gao[‡]

(*Department of Mathematical Sciences, University of Greenwich, London SE10 9LS*)

J.-M. Vanden-Broeck and J. J. S. Kandola

(*Department of Mathematics, University College London, London WC1E 6BT, UK*)

[Received 18 Nov 2019]

Summary

In this paper, we consider capillary-gravity waves propagating on the interface of two dielectric fluids under the influence of normal electric fields. The density of the upper fluid is assumed to be much smaller than the lower one. Linear and weakly nonlinear theories are studied. The connection to the results in other limit configurations is discussed. Fully nonlinear computations for travelling wave solutions are achieved via a boundary integral equation method. Periodic waves, solitary waves and generalised solitary waves are presented. The bifurcation of generalised solitary waves is discussed in detail.

1. Introduction

Electrohydrodynamics (EHD) is concerned with the interaction of charged fluid motion with electric fields. When performing experiments, it is much easier to artificially manipulate the electric field than it is to vary surface tension. EHD has numerous industrial chemical engineering applications, such as electrospray technology (**1**, **2**, **3**), enhanced heat transfer (**4**), cooling systems which make use of conducting fluids in high-power devices (**5**), coating processes (**6**, **7**), and so on. Two comprehensive reviews of advances and applications in EHD can be found in (**8**, **9**). EHD problems often concern an interface between two fluids, and hence an enhancement in the understanding of fluid dynamics benefits the engineering community. Research on EHD interfacial waves was first conducted by (**10**), who showed theoretically and experimentally that the interface between a dielectric and a conducting fluid can be destabilised by normal electric fields. It was followed by (**11**), who performed a linear stability analysis of interfacial flows under electric fields that are parallel to the undisturbed surface, and found that short waves can be regularised under such circumstances. Being inspired by these two earlier works, many authors considered the role of EHD in both stabilising and destabilising interfacial fluid configurations.

[‡] Email address for correspondence: t.gao@gre.ac.uk

Kelvin-Helmholtz and Rayleigh-Taylor instability were considered by (12) and (13, 14) respectively, where horizontal electric fields were shown to be capable of suppressing these instabilities. The results were achieved by using reduced model equations in (12, 13) and by direct numerical simulations in (14). Travelling waves of finite amplitude on capillary sheets under the influence of tangential electric fields were computed in (15) by a boundary integral equation method.

The problem of capillary-gravity travelling waves propagating under vertical electric fields in two-dimensions has been investigated by many authors for different configurations as summarised by (9). The general set up consists of two immiscible dielectric fluids with different electric permittivities, with an interface in between. To reduce the complexity of the problem, some assumptions were made in previous works. For example, (16, 17) assumed that the upper layer is much larger than the lower one. Under the long wave limits, Boussinesq-type models were derived and computed in the former literature whereas a boundary integral equation method was used to compute fully nonlinear solutions in the latter one. Another common assumption is to consider the case when one of the layers is a perfect conductor. Korteweg de-Vries (KdV), modified KdV, forced KdV and KdV-Benjamin-Ono equations were derived for long waves respectively by (18, 19, 20, 22) in the case of a layer of conducting fluid on the bottom and a dielectric on the top. The works were extended to three dimensions by (23, 24). On the other hand, in the case where the upper region is a conducting gas, (25, 26) computed fully nonlinear travelling solitary waves on a dielectric fluid of infinite and finite depth respectively as well as their dynamics based on a time-dependent hodograph transformation technique. To our knowledge, no fully nonlinear computations have been performed so far for the general set up of two dielectrics with two finite depth layers. This is the main focus of this work.

The rest of the paper is structured as follows. Detailed formulations are given in section 2, and followed by a linear theory in section 3 and a weakly nonlinear theory in section 4. The numerical scheme and the results are presented respectively in section 5 and 6. A conclusion is given in section 7.

2. Formulation

We consider the two-dimensional irrotational flow of an inviscid incompressible fluid of finite depth that is bounded below by an electrode and above by a hydrodynamically passive gas, which in turn is bounded above by another electrode (see figure 1). The fluid and the passive gas are assumed to be perfect dielectrics with permittivity ϵ_1 and ϵ_2 respectively. The problem can be formulated by using Cartesian coordinates with the y -axis directed vertically upwards and $y = 0$ at the mean level of the interface between the fluid and the gas. We take h as the undisturbed depth of the fluid, and h^+ as the undisturbed depth of the passive gas. The effects of gravity g and the surface tension σ are both included in the formulation. The interface between the fluid and the gas is a free surface whose unknown equation is denoted by $y = \zeta(x, t)$. A wavetrain is assumed to travel rightwards following the direction of the x -axis. We denote the voltage potential in the fluid and the gas by v and w respectively. Without loss of generality, we choose $v = 0$ on the bottom electrode. Continuity of the tangential component of the electric fields results in the condition that v and w are equal on the free-surface, up to an arbitrary constant, which without loss of generality we take to be zero. The potential on the upper electrode w is then a fixed parameter of the problem, which we denote by $w = E_0 h^+$. This choice of w on the upper

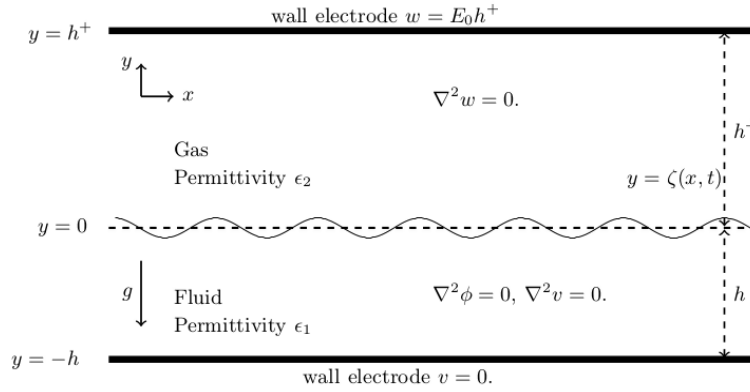


Fig. 1 Configuration of the problem. The gravity acts in the negative y -direction. We denote the equation of the unknown free surface by $y = \zeta(x, t)$.

electrode is chosen such that, in the case where $h^+ \rightarrow \infty$, the electric field approaches a uniform vertical electric field with strength E_0 . Since the fluid motion can be described by a velocity potential function $\phi(x, y, t)$, the governing equations can then be written as

$$\nabla^2 \phi = 0, \quad \text{for } -h < y < \zeta(x, t), \quad (2.1)$$

$$\nabla^2 v = 0, \quad \text{for } -h < y < \zeta(x, t), \quad (2.2)$$

$$\nabla^2 w = 0, \quad \text{for } \zeta(x, t) < y < h^+, \quad (2.3)$$

$$\zeta_t = \phi_y - \phi_x \zeta_x, \quad \text{on } y = \zeta(x, t), \quad (2.4)$$

$$\phi_y = 0, \quad \text{on } y = -h. \quad (2.5)$$

$$w = E_0 h^+, \quad \text{on } y = h^+, \quad (2.6)$$

$$v = 0 \quad \text{on } y = -h, \quad (2.7)$$

$$v_x + \zeta_x v_y = w_x + \zeta_x w_y \quad \text{on } y = \zeta(x, t), \quad (2.8)$$

$$v_y - \zeta_x v_x = \Lambda (w_y - \zeta_x w_x) \quad \text{on } y = \zeta(x, t), \quad (2.9)$$

and

$$\phi_t + \frac{1}{2} |\nabla \phi|^2 + g\zeta - \frac{T}{\rho} \frac{\zeta_{xx}}{(1 + \zeta_x^2)^{3/2}} + \sigma_e = B, \quad \text{on } y = \zeta(x, t), \quad (2.10)$$

where the subscripts denote partial derivatives, B is the Bernoulli constant and σ_e is the Maxwell stress given by

$$\sigma_e = -\frac{\epsilon_1}{\rho(1 + \zeta_x^2)} \left[\frac{1}{2} (1 - \zeta_x^2) (v_x^2 - v_y^2 - \Lambda (w_x^2 - w_y^2)) + 2\zeta_x (v_x v_y - \Lambda w_x w_y) \right] \quad (2.11)$$

with $\Lambda = \epsilon_2/\epsilon_1$ being the ratio of the permittivity from two layers. The last three terms of (2.10) are the forces due to gravity, surface tension, and the Maxwell stresses due to the electric field. Equations (2.4) and (2.5) are the kinematic boundary conditions on the

interface and bottom electrode respectively. The conditions (2.6) and (2.7) fix the electric potentials at the electrodes. Finally, continuity of the tangential components of the electric field and continuity of the normal component of the displacement field are given by (2.8) and (2.9) respectively. By making use of (2.8), (2.9), the Maxwell stress (2.11) can be simplified as

$$\sigma_e = \frac{\epsilon_1(\Lambda - 1)}{2\rho\Lambda(1 + \zeta_x^2)} \left[(\Lambda + \zeta_x^2)v_x^2 + (\Lambda\zeta_x^2 + 1)v_y^2 + 2(\Lambda - 1)v_xv_y\zeta_x \right]. \quad (2.12)$$

3. Linear theory

By choosing h , $\sqrt{h/g}$ and E_0 as the reference length, time and the strength of electric field, the bottom is at the level $y = -1$, and the system is still governed by the Laplace equations but with the dynamic boundary condition (2.10) becoming

$$\phi_t + \frac{1}{2}|\nabla\phi|^2 + \zeta + \sigma_e - \tau \frac{\zeta_{xx}}{(1 + \zeta_x^2)^{3/2}} = B \quad \text{on } y = \zeta(x, t), \quad (3.1)$$

and

$$\sigma_e = \frac{E_b(\Lambda - 1)}{2\Lambda(1 + \zeta_x^2)} \left[(\Lambda + \zeta_x^2)v_x^2 + (\Lambda\zeta_x^2 + 1)v_y^2 + 2(\Lambda - 1)v_xv_y\zeta_x \right], \quad (3.2)$$

where τ is the inverse Bond number and E_b is the inverse electric Bond number defined by

$$\tau = \frac{T}{\rho gh^2}, \quad E_b = \frac{\epsilon_1 E_0^2}{\rho gh}. \quad (3.3)$$

The boundary conditions on the voltage potential are now scaled to be

$$v = 0, \quad \text{on } y = -1, \quad (3.4)$$

$$w = \mathcal{R}, \quad \text{on } y = \mathcal{R}, \quad (3.5)$$

where $\mathcal{R} = h^+/h$. The kinematic conditions (2.4), (2.5), (2.8) and (2.9) remain unchanged. The trivial solution $\zeta(x, t) = 0$, $\phi(x, y, t) = 0$ gives rise to the following electric potentials

$$v = P\Lambda(y + 1), \quad (3.6)$$

$$w = P(y - \mathcal{R}) + \mathcal{R}, \quad (3.7)$$

where $P = \mathcal{R}/(\mathcal{R} + \Lambda)$. We linearise the system about the trivial solution by writing

$$\zeta(x, t) = \Re \left\{ A\epsilon e^{i(kx - \omega t)} \right\}, \quad (3.8)$$

$$\phi(x, y, t) = \Re \left\{ B\epsilon e^{i(kx - \omega t)} \cosh k(y + 1) \right\}, \quad (3.9)$$

$$v(x, y, t) = P\Lambda(y + 1) + \Re \left\{ C\epsilon e^{i(kx - \omega t)} \sinh k(y + 1) \right\}, \quad (3.10)$$

$$w(x, y, t) = P(y - \mathcal{R}) + \mathcal{R} + \Re \left\{ D\epsilon e^{i(kx - \omega t)} \sinh k(y - \mathcal{R}) \right\}, \quad (3.11)$$

where $|\epsilon| \ll 1$, ω is the angular frequency, k is the wavenumber, \Re represents the real part, and A , B , C , and D are constants to be found. For right-travelling waves, the wavenumber

k is always positive. The forms of these solutions ensure that (2.1), (2.2), (2.3), (2.5), (3.5) and (3.4) are satisfied. Substituting into (2.4) and (2.10) yields the following dispersion relation

$$c^2 = \left(\frac{1}{k} + \tau k \right) \tanh k - E_b \frac{P^2 (1 - \Lambda)^2 \tanh(k)}{\tanh(k) + \Lambda^{-1} \tanh(k\mathcal{R})}. \quad (3.12)$$

Here $c = \omega/k$ is the wave phase speed. It can be seen from equation (3.8) that if $c^2 < 0$ for some $k > 0$, then the configuration is linearly unstable to perturbations with wavenumber k . Noting that the term following E_b is positive for all $k > 0$, we can see that the vertical electric field is destabilising when the top electrode is held to a higher electric potential than the bottom one, while the effects of surface tension are stabilising. There are a variety of limiting configurations we will consider below.

1. In the case where the upper electrode is placed infinitely far away from the fluid ($\mathcal{R} \rightarrow \infty$), we find that

$$c_1^2 = \left(\frac{1}{k} + \tau k \right) \tanh k - E_b \frac{(1 - \Lambda)^2}{1 + \Lambda^{-1} \coth(k)}, \quad (3.13)$$

This configuration was seen in (16, 17), where the electric field at $y \rightarrow \infty$ is given by $w = E_0 y$.

2. In the particular case where the gas is a perfect conductor, as explored by (26), the governing equation (2.3) in the upper region is replaced by $w = \mathcal{R}$. This gives $w = 1$ for $\mathcal{R} = 1$. For any value of \mathcal{R} that is not unity, we rescale the voltage potentials such that $v = 0$ on the bottom electrode, and $w = 1$ on the upper electrode. Hence, the boundary conditions (2.8) and (2.9) for the electric fields on the interface are replaced by $v = 1$. The dispersion relation can be recovered from equation (3.12) by taking $\Lambda^{-1} \rightarrow 0$ (and hence $P\Lambda \rightarrow 1$), giving

$$c_2^2 = \left(\frac{1}{k} + \tau k \right) \tanh k - E_b. \quad (3.14)$$

3. In the case where the fluid is taken to be a conductor and the gas a dielectric, equation (2.2) is replaced by $v = 0$, and the boundary conditions (2.8) and (2.9) give $w = 0$ on $y = \zeta(x)$. Such a configuration was considered by (21, 24). For this case, E_b is no longer a valid non-dimensional constant (since $\epsilon_1 \rightarrow \infty$). We instead define

$$E_b^* = \frac{\epsilon_2 E_0^2}{\rho g h^3}. \quad (3.15)$$

The Bernoulli equation in this instance becomes

$$\begin{aligned} \phi_t + \frac{1}{2} |\nabla \phi|^2 + \zeta - \frac{E_b^*}{2(1 + \zeta_x^2)} \left[(1 - \zeta_x^2)(w_x^2 - w_y^2) + 4\zeta_x w_x w_y \right] \\ - \tau \frac{\zeta_{xx}}{(1 + \zeta_x^2)^{3/2}} = B \quad \text{on } y = \zeta(x, t), \end{aligned} \quad (3.16)$$

Using the expansions (3.8), (3.9) and (3.11) with $P = 1$ to satisfy $w = 0$ on the free surface, we find the linear dispersion relation

$$c_3^2 = \left(\frac{1}{k} + \tau k - E_b^* \coth(k\mathcal{R}) \right) \tanh k. \tag{3.17}$$

The similarity between equations (3.14) and (3.17) when $\mathcal{R} = 1$ is discussed in (26). On the other hand, when $\mathcal{R} \rightarrow \infty$, (3.17) reduces to

$$c_4^2 = \left(\frac{1}{k} + \tau k - E_b^* \right) \tanh k. \tag{3.18}$$

This set up was investigated in (22, 23).

Below, we consider the general case of dielectric-dielectric, as given by equation (3.12).

4. Weakly nonlinear theory

4.1 Finite long gas layer (shallow-shallow limit)

In this section, the weakly nonlinear theory is investigated under the KdV-scaling for long waves in the case where the upper region is of comparable size to the lower region, i.e. $\mathcal{R} = O(1)$. The dimensionless variables are defined as follows:

$$x = lx', \quad y = hy', \quad \zeta = a\zeta', \quad v = hE_0v', \quad w = hE_0w', \tag{4.1}$$

$$t = \frac{l}{\sqrt{gh}}t', \quad c = \sqrt{gh}c', \quad \phi = \frac{gla}{\sqrt{gh}}\phi', \tag{4.2}$$

where l is a typical horizontal lengthscale, a is a typical surface amplitude, and \sqrt{gh} is a typical wave velocity. The dashes are dropped for convenience. We also introduce

$$\alpha = \frac{a}{h}, \quad \beta = \left(\frac{h}{l} \right)^2, \tag{4.3}$$

that are the amplitude and depth parameters respectively. By using the dimensionless variables, the governing equations become

$$\beta\phi_{xx} + \phi_{yy} = 0, \quad \text{for } y < \alpha\zeta(x, t), \tag{4.4}$$

$$\beta v_{xx} + v_{yy} = 0, \quad \text{for } y < \alpha\zeta(x, t), \tag{4.5}$$

$$\beta w_{xx} + w_{yy} = 0, \quad \text{for } y > \alpha\zeta(x, t), \tag{4.6}$$

$$\zeta_t = \frac{1}{\beta}\phi_y - \alpha\phi_x\zeta_x, \quad \text{on } y = \alpha\zeta(x, t), \tag{4.7}$$

$$\phi_y = 0, \quad \text{on } y = -1. \tag{4.8}$$

$$w = \mathcal{R}, \quad \text{on } y = \mathcal{R}, \tag{4.9}$$

$$v = 0 \quad \text{on } y = -1, \tag{4.10}$$

$$v_x + \alpha\zeta_x v_y = w_x + \alpha\zeta_x w_y \quad \text{on } y = \alpha\zeta(x, t), \tag{4.11}$$

$$v_y - \alpha\beta\zeta_x v_x = \Lambda(w_y - \alpha\beta\zeta_x w_x) \quad \text{on } y = \alpha\zeta(x, t). \tag{4.12}$$

and

$$\phi_t + \frac{1}{2}(\alpha\phi_x^2 + \frac{\alpha}{\beta}\phi_y^2) + \zeta - \beta\tau \frac{\zeta_{xx}}{(1 + \alpha^2\beta\zeta_x^2)^{3/2}} + \sigma_e = B, \quad (4.13)$$

with

$$\sigma_e = \frac{E_b(\Lambda - 1)}{2\alpha\Lambda(1 + \alpha^2\beta\zeta_x^2)} \left(\beta v_x^2 (\Lambda + \alpha^2\beta\zeta_x^2) + v_y^2 (\alpha^2\beta\Lambda\zeta_x^2 + 1) + 2\alpha\beta(\Lambda - 1)v_x v_y \zeta_x \right) \quad (4.14)$$

where E_b is defined in (3.3). In the KdV-scaling, it is required that $\alpha = \beta = \epsilon$. We expand the functions in powers of ϵ by writing

$$\phi(x, y, t) = \phi_0 + \epsilon\phi_1 + \epsilon^2\phi_2 \dots, \quad (4.15)$$

$$\zeta(x, t) = \zeta_0 + \epsilon\zeta_1 + \epsilon^2\zeta_2 \dots, \quad (4.16)$$

$$v(x, y, t) = P\Lambda(y + 1) + \epsilon v_1 + \epsilon^2 v_2 \dots, \quad (4.17)$$

$$w(x, y, t) = P(y - \mathcal{R}) + \mathcal{R} + \epsilon w_1 + \epsilon^2 w_2 \dots, \quad (4.18)$$

where the leading order terms in (4.17) and (4.18) are derived in section 3. All the functions are expanded about $y = 0$ in the boundary conditions on the surface $y = \epsilon\zeta$. At order $O(1/\epsilon)$, the Bernoulli constant B is found to be

$$B = -\frac{1}{2}E_b P^2 \Lambda(1 - \Lambda). \quad (4.19)$$

By solving the Laplace equation (4.5) and (4.6) with (4.9) and (4.10), v_1 and w_1 can be written as

$$v_1 = (y + 1)A(x, t), \quad (4.20)$$

$$w_1 = (y - \mathcal{R})B(x, t). \quad (4.21)$$

The $O(\epsilon)$ balance in the boundary condition (4.12) gives us that $A(x, t) = \Lambda B(x, t)$. By making use of (4.11) at $O(\epsilon)$ to solve for $A(x, t)$ and collecting the terms of (4.7) and (4.13) at the leading order $O(\epsilon^0)$, the shallow water theory is obtained

$$\zeta_{0t} + \phi_{0_{xx}} = 0, \quad (4.22)$$

$$c_0^2 \zeta_{0x} + \phi_{0_{xt}} = 0, \quad (4.23)$$

with

$$c_0 = \sqrt{1 - \frac{E_b P^2 (1 - \Lambda)^2}{1 + \Lambda^{-1} \mathcal{R}}}, \quad (4.24)$$

which agrees with the long wave speed predicted by the dispersion relation (3.12) in the limit $k \rightarrow 0$.

In order to derive the KdV equation, we introduce

$$X = x - c_0 t, \quad T = \epsilon t. \quad (4.25)$$

Then we are required to simplify the boundary conditions (4.7) and (4.13) at $O(\epsilon)$. Solving the Laplace equation (4.4) combined with (4.8) for ϕ yields

$$\phi_1 = -\frac{(y+1)^2}{2}\phi_{0xx} + \psi_1(X, T), \tag{4.26}$$

$$\phi_2 = \frac{(y+1)^4}{24}\phi_{0xxxx} - \frac{(y+1)^2}{2}\psi_{1xx}, \tag{4.27}$$

Similarly, we solve (4.5) and (4.6) with (4.9)–(4.12) for v and w , and obtain

$$v_2 = \Lambda(y+1)V(X, T) - \frac{P(1-\Lambda)(y+1)^3}{6(1+\Lambda^{-1}\mathcal{R})}\zeta_{0xx}, \tag{4.28}$$

$$w_2 = (y-R)W(X, T) - \frac{P(1-\Lambda)(y-R)^3}{6(\mathcal{R}+\Lambda)}\zeta_{0xx}. \tag{4.29}$$

By summing the differentiation of (4.13) with respect to X and (4.7) multiplied by c_0 and making use of (4.11), (4.12), (4.24), ψ_1 , ζ_1 , V and W are all eliminated and the electrified Korteweg de-Vries equation is obtained

$$2c_0\zeta_{0T} + \delta\zeta_{0xxx} + \mu\zeta_0\zeta_{0x} = 0, \tag{4.30}$$

where

$$\delta = \frac{c_0^2}{3} - \tau + \frac{E_b P^2 \Lambda (1-\Lambda)^2 (\mathcal{R}^3 + \Lambda)}{3(\mathcal{R} + \Lambda)^2}, \tag{4.31}$$

$$\mu = 3c_0^2 - \frac{3E_b P^2 \Lambda (1-\Lambda)^3}{(\mathcal{R} + \Lambda)^2}. \tag{4.32}$$

Linearising (4.30) by taking the ansatz (3.8) for ζ , one recovers a relation between the angular frequency and wavenumber, which, when expanded about $k = 0$, agrees with the linear dispersion relation (3.12) up to order k^2 . In the absence of the electric field, (4.30) reduces to KdV equation for capillary-gravity waves. In the limit case where \mathcal{R} tends to infinity, the y coordinate in the upper layer should be scaled by l rather than h . Solution (4.21) is invalid since (4.6) becomes a standard Laplace equation for w . By elementary analysis as shown in (15), the y -derivative of w_1 is the Hilbert transform of the x -derivative, which finally results in a KdV-Benjamin-Ono equation. The details will be explained in the next subsection.

4.2 Infinitely wide gas layer (shallow-deep limit)

We denote the vertical Cartesian coordinate above the surface $y = \zeta(x)$ by Y . The new scaling is

$$x = lx', \quad y = hy', \quad \zeta = a\zeta', \quad v = hE_0v', \quad Y = lY', \tag{4.33}$$

$$w = lE_0w', \quad t = \frac{l}{\sqrt{gh}}t', \quad c = \sqrt{gh}c', \quad \phi = \frac{gla}{\sqrt{gh}}\phi'. \tag{4.34}$$

The governing equations (4.4), (4.5), (4.7), (4.8) and (4.10) remain unchanged. Equations (4.6), (4.9), (4.11) and (4.12) are respectively updated to

$$w_{xx} + w_{YY} = 0, \quad \text{for } Y > \alpha\sqrt{\beta}\zeta(x, t), \quad (4.35)$$

$$w_Y \rightarrow 1, \quad \text{as } Y \rightarrow \infty, \quad (4.36)$$

$$\sqrt{\beta}v_x + \alpha\sqrt{\beta}\zeta_x v_y = w_x + \alpha\sqrt{\beta}\zeta_x w_Y \quad \text{on } y = \alpha\zeta(x, t), \quad (4.37)$$

$$v_y - \alpha\beta\zeta_x v_x = \Lambda \left(w_Y - \alpha\sqrt{\beta}\zeta_x w_x \right) \quad \text{on } y = \alpha\zeta(x, t). \quad (4.38)$$

The fluid part of (4.13) has the same form but the Maxwell stress σ_e from (4.14) changes to

$$\sigma_e = \frac{E_b(\Lambda - 1)}{2\alpha(1 + \alpha^2\beta\zeta_x^2)} \left[w_x^2(1 + \alpha^2\beta\Lambda\zeta_x^2) + w_Y^2(\Lambda + \alpha^2\beta\zeta_x^2) - 2\alpha\sqrt{\beta}(\Lambda - 1)w_x w_Y \zeta_x \right]. \quad (4.39)$$

We still have $\alpha = \beta = \epsilon$. The asymptotic expansions for v and w are given by

$$v = \Lambda(y + 1) + \delta_1 v_1 + \dots, \quad (4.40)$$

$$w = Y + \delta_2 w_1 + \dots. \quad (4.41)$$

For the consistency of the boundary conditions (4.37) and (4.38), $\delta_1 = \delta_2 = \epsilon^{3/2}$ is required. Solving the Laplace problem (4.35) and making use of (4.37) and (4.38) yields at $O(\epsilon^{3/2})$

$$w_Y = \mathcal{H}[w_X] = -(1 - \Lambda)\mathcal{H}[\zeta_{0x}], \quad (4.42)$$

where \mathcal{H} is the Hilbert transform defined by a Cauchy principal value form as

$$\mathcal{H}[f](z) = \frac{1}{\pi} \text{P.V.} \int_{-\infty}^{\infty} \frac{f(\xi)}{\xi - z} d\xi. \quad (4.43)$$

After calculations similar to those in (22), we obtain a KdV-Benjamin-Ono equation

$$2\zeta_{0\tau} + 3\zeta_0\zeta_{0x} + \left(\frac{1}{3} - \tau\right)\zeta_{0xxx} + \bar{E}_b\Lambda(1 - \Lambda)^2\mathcal{H}[\zeta_{0xx}] = 0, \quad (4.44)$$

where $\bar{E}_b = \epsilon^{1/2}E_b$. The linear dispersion relation can be retrieved up to first two orders by expanding (3.13) in a power of k . We also note that equation (4.44) agrees with the Boussinesq system derived in (17).

5. Numerical scheme

In this section, we will explain the numerical method used to solve the fully nonlinear system of equations. We will use a boundary integral equation method, following closely the work in (17). The numerical method will be used to study waves of wavelength λ travelling at a constant speed c . Hence, it is advantageous to take a frame of reference moving with the wave, such that the problem is steady. We parameterise the interface $(X(s), Y(s))$ in (x, y) , where s is the arclength. We choose the origin such that $x = 0$ is at a point of symmetry of the wave (a crest or a trough), and $y = 0$ is again the mean level of the interface. We

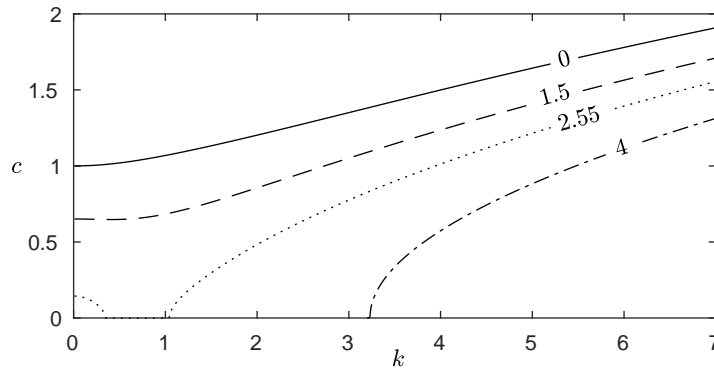


Fig. 2 Dispersion relation (3.12) with parameter values $\mathcal{R} = 2$, $\Lambda = 3$, $\tau = 0.5$. The values of E_b are shown in the figure.

choose $s = 0$ at the point $x = 0$, and denote the total arclength over a wavelength of the wave as b .

We wish to reduce the problem to a system of integro-differential equations. The complex velocity $U - iV$ is an analytic function of $z = x + iy$, and the no normal flow condition (2.5) on the bottom electrode $y = -1$ states that it is purely real on the real-axis. This allows us to reflect the flow across the boundary using the Schwarz reflection principle. Following (17), we conformally map the flow domain and its reflection in the z -plane $\{z = x + iy : -\lambda/2 < x < \lambda/2, -2 - \zeta(x) < y < \zeta(x)\}$ to an annulus Ω_1 in the t_1 -plane, via the function

$$t_1 = e^{-kiz} = e^{-kix} e^{ky}, \tag{5.1}$$

where $k = 2\pi/\lambda$ is the wavenumber. We apply Cauchy's integral equation to the function $U - iV$, taking the domain to be the annulus Ω_1 in the t_1 -plane. After some algebra, and making use of the assumed symmetry of the wave ($X(s) = -X(-s)$, $Y(s) = Y(-s)$ etc.), we find that the real part of the equation gives that

$$\begin{aligned} \frac{\pi}{k} U(s_0) &= \int_0^{b/2} \frac{\chi_1(U, V) (1 - R_- \cos \Theta_-) + \chi_2(U, V) R_- \sin \Theta_-}{1 + R_-^2 - 2R_- \cos \Theta_-} ds \\ &+ \int_0^{b/2} \frac{\chi_1(U, V) (1 - R_- \cos \Theta_+) - \chi_2(U, V) R_- \sin \Theta_+}{1 + R_-^2 - 2R_- \cos \Theta_+} ds \\ &- \int_0^{b/2} \frac{\chi_1(U, V) (1 - e^{2k} R_+ \cos \Theta_-) - \chi_2(U, V) R_+ \sin \Theta_-}{1 + R_+^2 - 2R_+ \cos \Theta_-} ds \\ &- \int_0^{b/2} \frac{\chi_1(U, V) (1 - R_+ \cos \Theta_+) + \chi_2(U, V) R_+ \sin \Theta_+}{1 + R_+^2 - 2R_+ \cos \Theta_+} ds \end{aligned} \tag{5.2}$$

where

$$R_- = e^{k(Y(s_0) - Y(s))}, \quad R_+ = e^{2k + k(Y(s_0) + Y(s))} \quad \Theta_{\pm} = k(X(s_0) \pm X(s)), \tag{5.3}$$

and

$$\chi_1(U, V) = U(s)X_s(s) + V(s)Y_s(s), \quad \chi_2(u, v) = U(s)Y_s(s) - V(s)X_s(s). \quad (5.4)$$

This is similar to equation (4.12) seen in (17). The above integral is a Cauchy-principal value.

Since v and w are scalar potentials of irrotational and incompressible vector fields, we can write them as the real parts of complex analytic functions,

$$F_1(z) = v(z) + i\xi(z), \quad F_2 = w(z) + i\nu(z), \quad (5.5)$$

where ξ and ν are the harmonic conjugates of v and w respectively. The harmonic potentials satisfy the Cauchy Riemann equations, given by

$$v_x = \xi_y, \quad v_y = -\xi_x, \quad w_x = \nu_y, \quad w_y = -\nu_x. \quad (5.6)$$

The derivatives of F_1 and F_2 are analytic, and hence making use of (5.6), we find that $\xi_x - i\xi_y$ and $\nu_x - i\nu_y$ are also analytic functions. Furthermore, the boundary conditions on the electrodes (2.6) and (2.7), combined with (5.6), imply that $\xi_y = 0$ and $\nu_y = 0$ on $y = -1$ and $y = R$ respectively. Hence, we can apply the Schwarz reflection principle to find the analytic continuation of $\xi_x - i\xi_y$ across $y = -1$ and $\nu_x - i\nu_y$ across $y = \mathcal{R}$.

We apply Cauchy's integral equation to the function $\xi_x - i\xi_y$, taking domain to be again the annulus Ω_1 in the t_1 -plane. Taking the real parts of this equation, one finds

$$\begin{aligned} \frac{\pi}{k}\xi_x(s_0) &= \int_0^{b/2} \frac{\chi_1(\xi_x, \xi_y)(1 - R_- \cos \Theta_-) + \chi_2(\xi_x, \xi_y)R_- \sin \Theta_-}{1 + R_-^2 - 2R_- \cos \Theta_-} ds \\ &+ \int_0^{b/2} \frac{\chi_1(\xi_x, \xi_y)(1 - R_- \cos \Theta_+) - \chi_2(\xi_x, \xi_y)R_- \sin \Theta_+}{1 + R_-^2 - 2R_- \cos \Theta_+} ds \\ &- \int_0^{b/2} \frac{\chi_1(\xi_x, \xi_y)(1 - e^{2k}R_+ \cos \Theta_-) - \chi_2(\xi_x, \xi_y)R_+ \sin \Theta_-}{1 + R_+^2 - 2R_+ \cos \Theta_-} ds \\ &- \int_0^{b/2} \frac{\chi_1(\xi_x, \xi_y)(1 - R_+ \cos \Theta_+) + \chi_2(\xi_x, \xi_y)R_+ \sin \Theta_+}{1 + R_+^2 - 2R_+ \cos \Theta_+} ds, \end{aligned} \quad (5.7)$$

To obtain a boundary integral equation relating to the electric potential in the gas region, we conformally map the upper region and its reflection across $y = \mathcal{R}$ to an annulus Ω_2 in the t_2 -plane via the mapping

$$t_2 = e^{kiz} = e^{kix} e^{-ky}. \quad (5.8)$$

We then apply Cauchy's integral equation to the function $\nu_x - i\nu_y$ in the annular region of

the t_2 -plane. Taking real parts of the integral equation, one finds that

$$\begin{aligned} \frac{\pi}{k} \nu_x(s_0) = & \int_0^{b/2} \frac{\chi_1(\nu_x, \nu_y) \left(1 - \hat{R}_- \cos \hat{\Theta}_-\right) - \chi_2(\nu_x, \nu_y) \hat{R}_- \sin \hat{\Theta}_-}{1 + \hat{R}_-^2 - 2\hat{R}_- \cos \hat{\Theta}_-} ds \\ & + \int_0^{b/2} \frac{\chi_1(\nu_x, \nu_y) \left(1 - \hat{R}_- \cos \hat{\Theta}_+\right) + \chi_2(\nu_x, \nu_y) \hat{R}_- \sin \hat{\Theta}_+}{1 + \hat{R}_-^2 - 2\hat{R}_- \cos \hat{\Theta}_+} ds \\ & - \int_0^{b/2} \frac{\chi_1(\nu_x, \nu_y) \left(1 - \hat{R}_+ \cos \hat{\Theta}_-\right) + \chi_2(\nu_x, \nu_y) \hat{R}_+ \sin \hat{\Theta}_-}{1 + \hat{R}_+^2 - 2\hat{R}_+ \cos \hat{\Theta}_-} ds \\ & - \int_0^{b/2} \frac{\chi_1(\nu_x, \nu_y) \left(1 - \hat{R}_+ \cos \hat{\Theta}_+\right) - \chi_2(\nu_x, \nu_y) \hat{R}_+ \sin \hat{\Theta}_+}{1 + \hat{R}_+^2 - 2\hat{R}_+ \cos \hat{\Theta}_+} ds, \end{aligned} \quad (5.9)$$

where

$$\hat{R}_- = e^{-k(Y(s_0)-Y(s))}, \quad \hat{R}_+ = e^{2k\mathcal{R}-k(Y(s_0)+Y(s))}, \quad \hat{\Theta}_\pm = k(X(s_0) \pm X(s)). \quad (5.10)$$

Consider a wave whose interface has a length b per wavelength λ . We discretise s into N equally spaced meshpoints s_i over a half wavelength, given by

$$s_i = \frac{(i-1)b}{2N}, \quad i = 1, 2, \dots, N. \quad (5.11)$$

Denote the $N-1$ midpoints as s_i^m where

$$s_i^m = \frac{s_i + s_{i+1}}{2}, \quad i = 1, 2, \dots, N-1. \quad (5.12)$$

The values of X_s, Y_s, U, V, ν_x and ν_y at each meshpoint are unknown. One can express the derivatives of v and w in terms of ξ and ν using equations (5.6) One can then find ξ_x and ξ_y in terms of ν_x and ν_y by rearranging the boundary conditions (2.8) and (2.9), to find that

$$\xi_x = (1 + \eta_x^2)^{-1} [\nu_y \eta_x (\Lambda - 1) + \nu_x (\eta_x^2 + \Lambda)], \quad (5.13)$$

$$\xi_y = (1 + \eta_x^2)^{-1} [\nu_y (\eta_x^2 \Lambda + 1) + \nu_x \eta_x (\Lambda - 1)]. \quad (5.14)$$

Since we are seeking periodic solutions, we can express the unknowns in a Fourier series, which we truncate after a finite number of terms as follows

$$\begin{aligned} X_s(s) &= \sum_{n=0}^N a_n \cos\left(\frac{2\pi n}{b}s\right), & Y_s(s) &= \sum_{n=1}^{N-1} b_n \sin\left(\frac{2\pi n}{b}s\right), \\ U(s) &= \sum_{n=0}^N c_n \cos\left(\frac{2\pi n}{b}s\right), & V(s) &= \sum_{n=1}^{N-1} d_n \sin\left(\frac{2\pi n}{b}s\right), \\ \nu_x(s) &= \sum_{n=0}^N e_n \cos\left(\frac{2\pi n}{b}s\right), & \nu_y(s) &= \sum_{n=1}^{N-1} f_n \sin\left(\frac{2\pi n}{b}s\right). \end{aligned} \quad (5.15)$$

Fixing λ , τ , \mathcal{R} , E_b , Λ , and the amplitude A , we have $6N + 1$ unknowns: the coefficients of the Fourier series a_n, \dots, f_n , the Bernoulli constant B , the length of the wave b , the value $H = Y(0)$ and the wavespeed c . We satisfy the boundary integral equations (5.2), (5.7) and (5.9) at the midpoints s_i^m . The integrals are Cauchy-principle value, and are evaluated using the trapezoidal rule. This results in $3N - 3$ discrete equations. By the definition of arclength, we have that

$$X_s(s)^2 + Y_s(s)^2 = 1. \quad (5.16)$$

Furthermore, the boundary condition (2.4) can be written as

$$U(s)Y_s(s) - V(s)X_s(s) = 0. \quad (5.17)$$

We fix the amplitude by satisfying

$$A = Y(s_N) - Y(s_1), \quad (5.18)$$

and the mean depth of the interface to 0 by setting

$$\int_0^{b/2} Y(s)X_s(s) \, ds = 0. \quad (5.19)$$

We define the wavespeed c as the average horizontal velocity for a constant value of $y = a$,

$$c = \frac{2}{\lambda} \int_0^{\lambda/2} U \, dx. \quad (5.20)$$

Irrotationality of the velocity field implies that the equation (5.20) is independent of the value a . One can then show

$$c = \frac{2}{\lambda} \int_0^{b/2} U(s)X_s(s) + V(s)Y_s(s) \, ds. \quad (5.21)$$

We fix the wavelength λ via the equation

$$\lambda = 2 \int_0^{b/2} X_s(s) \, ds. \quad (5.22)$$

We need to fix the potential difference between the two electrodes. In the previous sections, we fixed the potential difference (after non-dimensionalisation) across the electrodes to be \mathcal{R} . This is an integral condition, which for a fixed $x = a$, is given by

$$\mathcal{R} = \int_0^{\eta(x)} v_y \, dy + \int_{\eta(x)}^{\mathcal{R}} w_y \, dy. \quad (5.23)$$

However, this condition is numerically expensive to enforce, since it involves evaluating terms within the fluid and gas domains. It is numerically easier to fix the variation in the complex conjugates of v and w across a wavelength for a fixed y . As with the velocity field, the electric fields are both irrotational and incompressible, and hence this integral is independent on the value of y . Hence, we fix a constant p , defined as

$$p = 2 \int_0^{b/2} \nu_x X_s + \nu_y Y_s \, dx. \quad (5.24)$$

We choose $p = -P\lambda$, where P is defined in section 3 of the paper. This choice of p ensures that, for an undisturbed surface, the potential difference between the two electrodes is exactly equal to \mathcal{R} , and hence numerical results in the following section agree with the linear theory (for example, the dispersion relation (3.12)) of section 3 for small values of the amplitude. The potential difference of a solution can then be obtained by evaluating the integral on the right-hand side of equation (5.23). Finally, Bernoulli's equation, written in terms of the unknowns (5.15) and satisfied at $s = s_i$, becomes

$$\frac{1}{2}(U^2 + V^2) + \int_0^{s_i} Y_s(s) ds + \tau (X_s Y_{ss} - Y_s X_{ss}) + \sigma_e = B \tag{5.25}$$

As stated before, satisfying the three Cauchy integrals (5.2), (5.7) and (5.9) at the midpoints s_i^m results in $3N - 3$ equations. We satisfy equations (5.16) and (5.25) at the meshpoints s_i , and (5.17) at the midpoints s_i^m . This results in a further $3N - 1$ equations. Finally, we satisfy (5.18), (5.19), (5.20), (5.22) and (5.24), resulting in $6N + 1$ equations for the $6N + 1$ unknowns. We solve this discrete nonlinear system via Newton's method, where we terminate the iterative procedure once the L^∞ norm of the residuals is $O(10^{-11})$.

As well as periodic waves, we also wish to compute solitary waves. One could rewrite the integrals (5.2), (5.7) and (5.9) by using a different conformal mapping to map the domains onto finite width strips in the t -plane. Another commonly used method (for example, see (27)) is to approximate solitary waves as long periodic waves. This is the method we shall adopt in this paper. When computing solitary waves, we replace (5.19) with a flat far-field condition

$$Y(s_1) = 0. \tag{5.26}$$

In the following section, we discuss the numerical results of periodic waves, solitary waves and generalised solitary waves.

6. Numerical results

We have tested the numerical method for a variety of parameter values. Most of the results that follow will have the following parameters:

$$E_b = 1.5, \quad \Lambda = 3, \quad \mathcal{R} = 2. \tag{6.1}$$

The value of δ and μ from equation (4.31) in this instance is given by $\delta = 0.5637 - \tau$ and $\mu = 1.9632$. Hence, the value of δ changes sign according to the value of τ . Three different regimes are possible depending on the value of τ ,

1. when $\tau < 0.1315$, the fluid system is destabilised for some wavenumber.
2. when $0.1315 < \tau < 0.5637$, the linear phase speed admits a positive minimum. The associated KdV equation (4.30) admits elevation soliton solutions.
3. when $\tau > 0.5637$, the linear phase speed is monotonically increasing. The associated KdV equation (4.30) admits depression soliton solutions.

The minimum of the phase speed equals zero when $\tau = 0.1315$. When $\tau < 0.1315$, we find that the flow configuration is unstable (the value of c^2 in the dispersion relation (3.12) is negative for some values of k). Meanwhile, for τ being above (below) the critical value 0.5637, δ is negative (positive) and the KdV equation (4.30) admits depression (elevation)

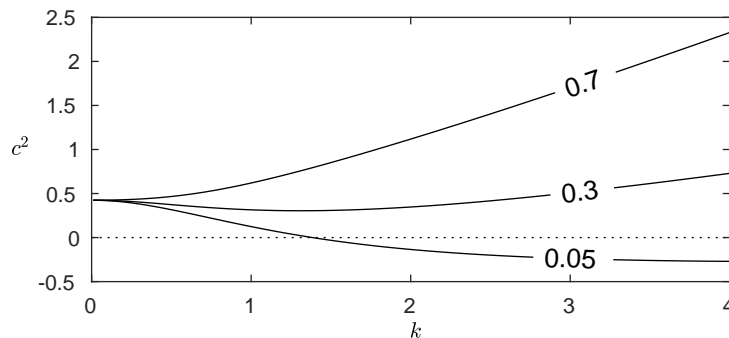


Fig. 3 Dispersion relation (3.12) with the parameter values given by equation (6.1), with varying values of τ (as shown in the figure). When the curve goes below $c^2 = 0$ (given by the dotted line), the configuration is linearly unstable.

soliton solutions. Figure 3 shows the dispersion relation for values of τ in these three regimes. In the critical case $\tau = 0.5637$, the standard KdV equation is invalid as the dispersive term from (4.30) vanishes. A fifth-order KdV equation can be derived under such circumstance, which is not explored in this work. Varying the values of the parameters shown in equation (6.1) changes the values of τ for which these regime changes occur. In particular, increasing E_b increases the value of τ for which there exists unstable modes. This is due to the electric field destabilising the flow, while the surface tension is a stabilising force.

First, let us explore the regime where the linear phase speed is monotonic. We compare a depression KdV soliton satisfying equation (4.30) with a solution to the full Euler equations with the parameter values given by equation (6.1) and $\tau = 1.2$. As shown in Figure 4, the agreement is very satisfactory. Such convincing results ensure that our codes based on the numerical scheme are correctly composed. We also show in the figure a full Euler solution with the same parameter values, except $E_b = 0$. It can be seen that the solution with the electric field is less steep than the gravity-capillary solitary wave. While there is little difference in the profiles, the effect on the speed of the wave is dramatic. The $E_b = 0$ solution has $c = 0.915$, while the $E_b = 1.5$ solution has $c = 0.5578$. Increasing E_b further, one finds that the speed of the soliton approaches zero. This is shown in figure 5, where we have fixed $A = -0.2$ and allowed E_b to vary. A relationship between E_b and c is found. The points (a) and (b) on the figure correspond to the solutions shown in figure 4.

Next, consider the regime, where the dispersion relation experiences a minimum $c = c^* > 0$. We compute solitary wavepackets in the full Euler regime. By (29), these solutions can be approximated by the associated Nonlinear Schrödinger (NLS) Equation's solitary wave solution at small amplitude. Both elevation and depression solitary wave packets bifurcate from the minimum of the dispersion relation by (30). Without any knowledge on the NLS, an alternative approach to discover these solitary waves is to apply an artificial Gaussian pressure to the free-surface, and find solutions with $c < c^*$ which are perturbations to the uniform stream (characterised by small amplitudes). We then follow the branch of solutions with an artificial pressure to larger amplitudes. Once a suitably large solution is found, one can use this solution as an initial guess for a solitary wave packet with no artificial pressure. This trick has been used in previous literature, for example in (31). Here we only show the

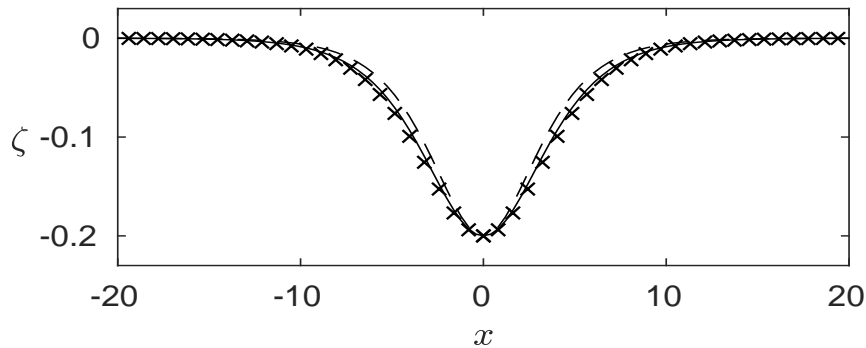


Fig. 4 Comparison of computations for a depression soliton with $A = -0.2$, $\lambda = 80$, $E_b = 1.5$, $\Lambda = 3$, $\mathcal{R} = 2$, and $\tau = 1.2$ by the full Euler (solid line) and by (4.30) (crosses). The dashed curve is a full Euler solution with $E_b = 0$.

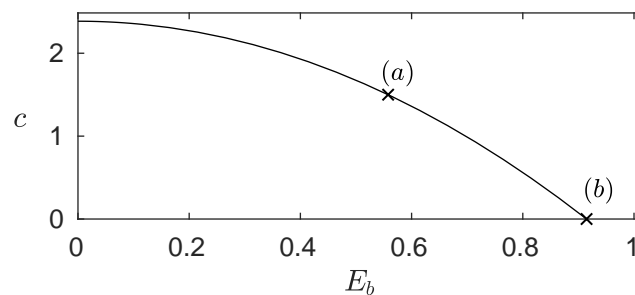


Fig. 5 A branch of depression solitons with $A = -0.2$, $\Lambda = 3$, $\mathcal{R} = 2$, and $\tau = 1.2$. We see that, as E_b is increased, the speed of the wave decreases, until eventually no depression soliton solutions are found for $E_b > 2.39$. The points (a) and (b) correspond to the solid and dashed curve in figure 4 respectively.

existence of the wavepackets as presented in Figure 6. The rigorous analysis of these waves requires a future study on the NLS.

We seek non-resonant periodic waves with $\tau = 0.4$ by using a linear solution as the initial guess in Newton’s method. The continuation over the amplitude is shown in the left graph of Figure 7. The corresponding wave profiles are plotted on the right. Highly nonlinear solution possess a sharp trough and a broad crest. We follow to find resonant periodic waves with the same inverse Bond number and $A = 0.05$ by choosing the value of λ from (3.12) such that the solution experiences second, third, fourth and fifth mode resonance respectively as presented in Figure 8 (a)-(d).

Additionally, due to the presence of a phase speed minimum, resonance of the long wave (elevation soliton as predicted by the associated KdV) with a short wave occurs at zero wavenumber resulting in non-decaying oscillatory ripples in the tail. These solutions are called generalised solitary wave, and they can be found numerically by extending the

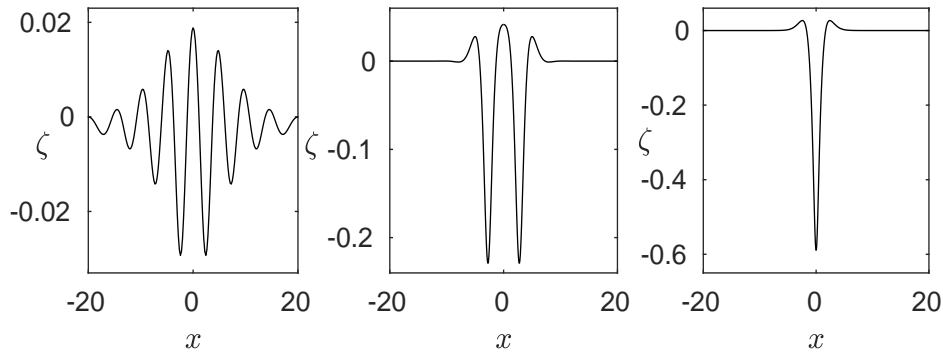


Fig. 6 Solitary wavepacket profiles. All have parameter values given by equation (6.1), and $\tau = 0.3$. The figures on the left and in the center are elevation solitary waves, while the figure on the right is a depression solitary wave.

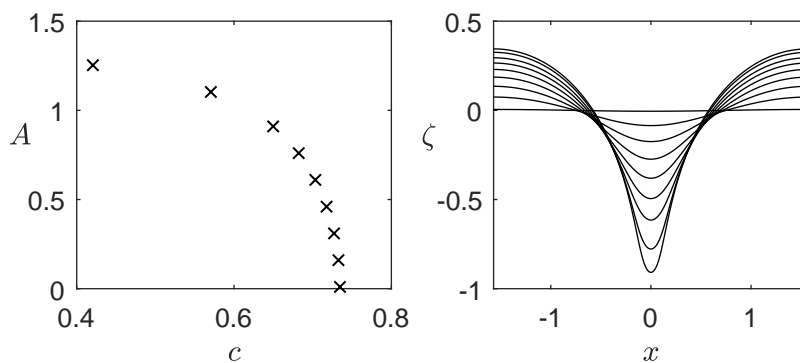


Fig. 7 Computations for periodic waves with $\lambda = \pi$, $E_b = 1.5$, $\Lambda = 3$, $\mathcal{R} = 2$, $\tau = 0.4$ and various values of A . The figure on the left is the amplitude-speed diagram. The associated wave profiles are shown in the rightmost figure.

wavelength of a periodic solution with speed greater than the long wave speed. As one increases the wavelength more ripples appear in the far field. We stop the numerical procedure when there is minimal change in the profile as the wavelength is further increased. Further by a continuation on the branch, a complete diagram is obtained for $\tau = 0.4$ as presented in Figure 9. The wavelength chosen here is 69.83, and the corresponding phase speed from the linear dispersion relation (3.12) is about 0.6501. When the amplitude is close to zero, the branch approaches the predicted phase speed marked by a circle. The associated long wave speed from (4.24) is 0.6512 marked by a diamond. The difference between the values stems from the fact that we have approximated generalised solitary waves with solutions of finite wavelength. The gap between the circle and the diamond is decreased as the wavelength is increased. In the limit of long wave, these two points collapse. Two typical wave profiles are plotted on the right of the figure. Despite of the

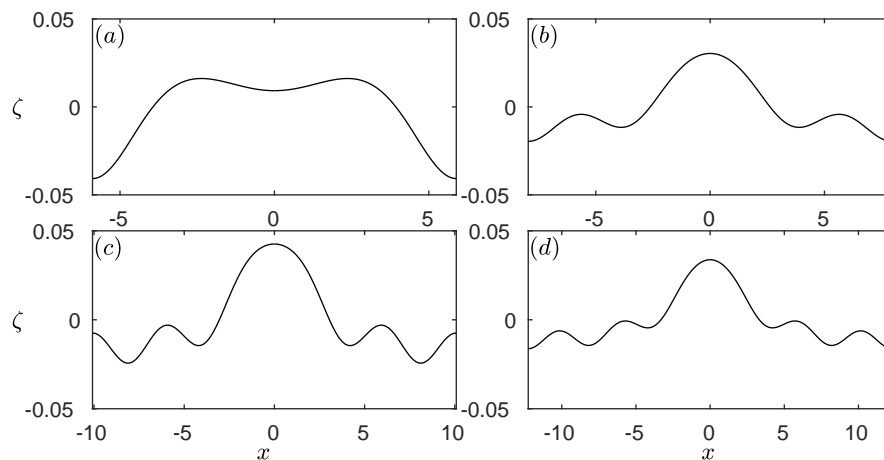


Fig. 8 Typical wave profiles of resonant periodic solutions with $E_b = 1.5$, $\Lambda = 3$, $\mathcal{R} = 2$, $\tau = 0.4$ and $A = 0.05$. The value of λ is chosen such that the solution experiences second, third, fourth and fifth mode resonance respectively for graphs (a)-(d).

almost flat surface in the tail, profile (a) is not an embedded soliton since there are still tiny ripples of size comparable to the numerical error from Newton's method.

7. Conclusion

In conclusion, we have presented linear, weakly nonlinear and fully nonlinear solutions to the generalised problem of interfacial waves between a fluid and gaseous dielectric, in the presence of a vertical electric field. The linear regime under various settings has been illustrated and summarised. Korteweg de-Vries equation has been derived for long waves. A valid numerical scheme of boundary integral equation has been introduced for fully nonlinear computations. Periodic, solitary and generalised solitary waves have been computed. The bifurcation of generalised solitary waves has been discussed in detail.

Acknowledgement

The work was initiated by a MSc dissertation for University College London by J. J. S. K. and achieved during a collaborative research visit of A. D. at University of Bath sponsored by the QJMAM fund for applied mathematics (T. G.). A.D. was also supported under grant EP/M507970/1. JMVDB was supported by EPSRC under grant EP/N018559/1.

References

1. G. I. Taylor, Disintegration of Water Droplets in an Electric Field. *Proc. Roy. Soc. A*, **280** (1964) 383–397.
2. G. I. Taylor, The force exerted by an electric field on a long cylindrical conductor. *Proc. Roy. Soc. A*, **291** (1965) 145–158.
3. G. I. Taylor & M. D. Van Dyke, Electrically Driven Jets. *Proc. Roy. Soc. A*, **313** (1969) 453–475.

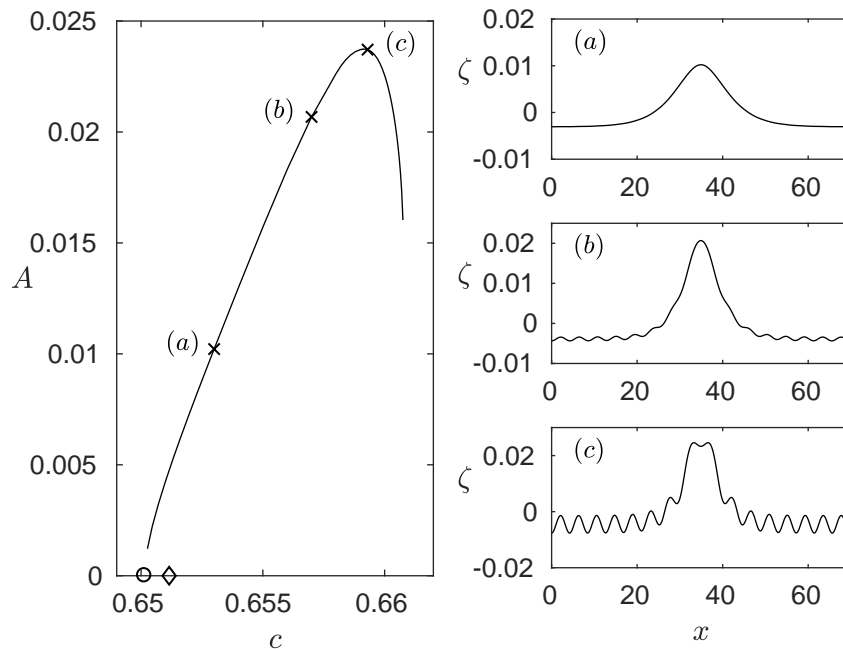


Fig. 9 The figure on the left is an amplitude-speed diagram of the generalised elevation solitary waves with $E_b = 1.5$, $\tau = 0.4$, $\mathcal{R} = 2$, $\Lambda = 3$ and $\lambda = 69.83$. The phase speed predicted by the dispersion relation is marked as a circle on the axis. The long wave speed is marked as a diamond. The corresponding profiles for the waves which are marked by a cross in the left graph are shown in the right three figures.

4. T. B. Jones, Electrohydrodynamically enhanced heat transfer in liquids—a review. *Advances in heat transfer*. **14** (1979) 107–148.
5. U. Ghoshal & A. C. Miner, Cooling of high power density devices by electrically conducting fluids. *U.S. Patent* (2003) 6,658,861.
6. S. F. Kistler & P. M. Schweizer, *Liquid film coating - scientific principles and their technological implications*, Chapman and Hall, 1997.
7. E. M. Griffing, S. G. Bankoff, M. J. Miksis & R. A. Schluter, Electrohydrodynamics of thin flowing films, *J. Fluids Eng.* **128** (2006) 276–283.
8. X. Chen, & J. Cheng, and X. Yin. Advances and applications of electrohydrodynamics. *Chin. Sci. Bull.* **48** (2003): 1055–1063.
9. D. T. Papageorgiou, Film Flows in the Presence of Electric Fields. *Ann. Rev. Fluid Mech.* **51** (2019) 155–187.
10. G. Taylor & A. McEwan, The stability of a horizontal fluid interface in a vertical electric field, *J. Fluid Mech.* **22** (1965) 1–15.
11. J. R. Melcher & W. J. Schwarz, Interfacial relaxation overstability in a tangential electric field, *Phys. Fluids* **11** (1968) 2604–2616.
12. N. M. Zubarev & E. Kochurin, Nonlinear dynamics of the interface between fluids at

- the suppression of Kelvin-Helmholtz instability by a tangential electric field, *JETP letters* **104** (2016) 275–280.
13. L. L. Barannyk & D. T. Papageorgiou & P. G. Petropoulos, Suppression of Rayleigh-Taylor instability using electric fields, *Math. Comp. Simul.* **82** (2012) 1008–1016.
 14. R. Cimpeanu, D. T. Papageorgiou, P. G. Petropoulos, On the control and suppression of the Rayleigh-Taylor instability using electric fields, *Phys. Fluids* **26** (2014) 022105.
 15. D. T. Papageorgiou, J.-M. Vanden-Broeck, Large-amplitude capillary waves in electrified fluid sheets, *J. Fluid Mech.* **508** (2004) 71–88.
 16. D. T. Papageorgiou, P. G. Petropoulos & J.-M. Vanden-Broeck, Gravity capillary waves in fluid layers under normal electric fields. *Phys. Rev. E*, **72** (2005) 051601.
 17. D. T. Papageorgiou, & J.-M. Vanden-Broeck, Numerical and analytical studies of nonlinear gravity–capillary waves in fluid layers under normal electric fields. *IMA J. Appl. Math.*, **72** (2006) 832–853.
 18. C. Easwaran, Solitary waves on a conducting fluid layer, *Phys. Fluids* **31** (1988) 3442–3443.
 19. T. Perelman, A. Fridman, M. Eliashevich, Modified Korteweg-de Vries equation in electrohydrodynamics, *Sov. Phys. JETP* **66** (1974) 1316–1323.
 20. M. J. Hunt, & J.-M. Vanden-Broeck, A study of the effects of electric field on two-dimensional inviscid nonlinear free surface flows generated by moving disturbances. *J. Eng. Math.*, **92** (2015) 1–13.
 21. P. Hammerton, Existence of solitary travelling waves in interfacial electrohydrodynamics, *Wave Motion* **50** (4) (2013) 676–686.
 22. H. Gleeson, P. Hammerton, D. Papageorgiou, J.-M. Vanden-Broeck, A new application of the Korteweg-de Vries Benjamin-Ono equation in interfacial electrohydrodynamics, *Phys. Fluids* **19** (2007) 031703.
 23. M. Hunt, J.-M. Vanden-Broeck, D. T. Papageorgiou, E. Părău, Benjamin-Ono Kadomtsev–Petviashvili’s models in interfacial electro-hydrodynamics, *Eur. J. Mech.-B/Fluids* **65** (2017) 459–463.
 24. Z. Wang, Modelling nonlinear electrohydrodynamic surface waves over three-dimensional conducting fluids, *Proc. Roy. Soc. A* **473** (2200) (2017) 20160817.
 25. T. Gao, P. A. Milewski, D. T. Papageorgiou, & J.-M. Vanden-Broeck. Dynamics of fully nonlinear capillary–gravity solitary waves under normal electric fields. *J. Eng. Math.* **108** (2018) 107–122.
 26. T. Gao, A. Doak, J.-M. Vanden-Broeck & Z. Wang, Capillary-gravity waves on a dielectric fluid of finite depth under normal electric field, *Eur. J. Mech. B* **77** (2019) 98–107.
 27. F. Dias, Capillary–gravity periodic and solitary waves. *Phys. Fluids*, **6**(7) (1994) 2239–2241.
 28. Z. Wang, Stability and dynamics of two-dimensional fully nonlinear gravity–capillary solitary waves in deep water. *J. Fluid Mech.*, **809**, 530–552.
 29. F. Dias & G. Iooss, Capillary-gravity solitary waves with damped oscillations. *Physica D*, **65**(4) (1993) 399–423.
 30. G. Iooss & P. Kirmann, Capillary-gravity waves on the free surface of an inviscid fluid of infinite depth: existence of solitary waves. *Arch. Rat. Mech. Anal.* (1996) **136**, 1–19.

31. J.-M. Vanden-Broeck & F. Dias, Gravity-capillary solitary waves in water of infinite depth and related free-surface flows. *J. Fluid Mech.*, **240** (1992) 549–557.